Published in final edited form as:
Toxicol Lett. 2015 April 2; 234(1): 40–49. doi:10.1016/j.toxlet.2015.02.004.

Endoplasmic reticulum stress and oxidative stress are involved in ZnO nanoparticle-induced hepatotoxicity

Xia Yang[a], **Huali Shao**[a], **Weirong Liu**[a], **Weizhong Gu**[a], **Xiaoli Shu**[a], **Yiqun Mo**[b], **Xuejun Chen**[a], **Qunwei Zhang**[b], and **Mizu Jiang**[a]

[a]Department of Gastroenterology, Children's Hospital, Zhejiang University School of Medicine, Hangzhou, Zhejiang, P. R. of China

[b]Department of Environmental and Occupational Health Sciences, School of Public Health and Information Sciences, University of Louisville, Louisville, Kentucky, USA

Abstract

Zinc oxide nanoparticles (Nano-ZnO) are widely used in sunscreens, clothes, medicine and electronic devices. However, the potential risks of human exposure and the potential for adverse health impacts are not well understood. Previous studies have demonstrated that exposure to Nano-ZnO caused liver damage and hepatocyte apoptosis through oxidative stress, but the molecular mechanisms that are involved in Nano-ZnO-induced hepatotoxicity are still unclear. Endoplasmic reticulum (ER) is sensitive to oxidative stress, and also plays a crucial role in oxidative stress-induced damage. Previous studies showed that ER stress was involved in many chemical-induced liver injuries. We hypothesized that exposure to Nano-ZnO caused oxidative stress and ER stress that were involved in Nano-ZnO-induced liver injury. To test our hypothesis, mice were gavaged with 200 mg/kg or 400 mg/kg of Nano-ZnO once a day for a period of 90 days, and blood and liver tissues were obtained for study. Our results showed that exposure to Nano-ZnO caused liver injury that was reflected by focal hepatocellular necrosis, congestive dilation of central veins, and significantly increased alanine transaminase (ALT) and aspartate transaminase (AST) levels. Exposure to Nano-ZnO also caused depletion of glutathione (GSH) the liver tissues. In addition, our electron microscope results showed that ER swelling and ribosomal degranulation were observed in the liver tissues from mice treated with Nano-ZnO. The mRNA expression levels of ER stress-associated genes (grp78, grp94, pdi-3, xbp-1) were also up-regulated in Nano-ZnO-treated mice. Nano-ZnO caused increased phosphorylation of RNA-dependent protein kinase-like ER kinase (PERK) and eukaryotic initiation factor 2α (eIF2α). Finally, we found that exposure to Nano-ZnO caused increased ER stress-associated apoptotic protein levels, such as caspase-3, caspase-9, caspase-12, phosphorylation of JNK, and CHOP/

Address Correspondence To: Mizu Jiang, MD, PhD, Department of Gastroenterology, Children's Hospital, Zhejiang University School of Medicine. Hangzhou 310003, Zhejiang, P. R. of China. mizu@zju.edu.cn. **or**, Qunwei Zhang, MD, PhD, Department of Environmental Health and Occupational Health Sciences, School of Public Health and Information Sciences, University of Louisville. 485 E. Gray Street, Louisville, KY 40202. Tel: (502)852-7200 Fax: (502)852-7246 Qunwei.Zhang@louisville.edu.

GADD153, and up-regulation of pro-apoptotic genes (chop and bax). These results suggest that oxidative stress and ER stress-induced apoptosis are involved in Nano-ZnO-induced hepatotoxicity in mice.

Keywords

Nano-ZnO; oxidative stress; endoplasmic reticulum stress; apoptosis; liver injury

1. Introduction

With the development of nanotechnology, nanoparticles have become widely utilized in consumer products with their unique properties and excellent qualities. Among the various engineered nanoparticles, zinc oxide nanoparticles (Nano-ZnO) are one of the most widely used metal nanoparticles. They have been widely used in cosmetics, sunscreens, food additives, clothing, electronics and medical products (Aydin Sevinc and Hanley, 2010; Rasmussen et al., 2010; Su et al., 2010; Umrani and Paknikar, 2014). Due to the increased production and use of Nano-ZnO, the potential toxic effects of Nano-ZnO can not be neglected (Schilling et al., 2010; Service, 2003). Therefore, it is necessary to understand and evaluate the potential toxic effects of Nano-ZnO in order to avoid their adverse effects on biological system and human health.

Previous studies have shown that Nano-ZnO mainly accumulate in the liver, pancreas, kidney, heart, spleen and lungs after they entered the body through skin, respiratory tract and gastrointestinal tract exposures (Baek et al., 2012; Baky et al., 2013; Cho et al., 2011; Cho et al., 2013; Chuang et al., 2014; Pasupuleti et al., 2012; Seok et al., 2013; Sharma et al., 2012a; Sharma et al., 2012b; Wang et al., 2006). In this study, we mainly focused on the hepatotoxic effects of Nano-ZnO and the potential mechanisms. Previous studies have demonstrated that Nano-ZnO induced apoptosis in mouse liver through oxidative stress after oral exposure to Nano-ZnO for 14 days (Sharma et al., 2012b). Nano-ZnO also caused apoptosis in human hepatocytes (HepG2), human lung epithelial cells and some human cancer cells through reactive oxygen species (ROS) production (Akhtar et al., 2012; Huang et al., 2010; Premanathan et al., 2011; Sharma et al., 2012a). These studies suggest that ROS generation may be involved in Nano-ZnO-induced toxic effects.

Endoplasmic reticulum (ER) is an organelle responsible for protein folding and assembly, protein post-translational modification, lipid biosynthesis, vesicular trafficking, and cellular calcium storage (Michalak, 2010). ER is abundant in hepatocytes, and the mixed-function oxidase system in the ER plays a crucial role in the detoxification process in the liver. ER is sensitive to changes of intracellular homeostasis. Oxidative stress, the inhibition of protein glycosylation, a reduction in disulfide bond formation, calcium depletion and accumulation of unfolded proteins in the ER lumen may disrupt the ER function, and trigger the unfolded protein response (UPR), also known as “ERstress”, a series of signal transduction pathways from ER to the nucleus designed to restore ER homeostasis (Ron and Walter, 2007). Proper ER function is essential to cell survival, and perturbation of its function induces cellular damage and results in apoptosis. ER has been shown to play an important role in a number

of liver diseases, such as drug- and alcohol-induced liver injury, nonalcoholic fatty liver disease, chronic viral hepatitis, and hepatocellular carcinoma (Malhi and Kaufman, 2011).

ER stress is activated by three signaling proteins named inositol-requiring protein 1α (IRE1α), protein kinase RNA (PKR), and activating transcription factor 6 (ATF6) (Walter and Ron, 2011; Wu and Kaufman, 2006). Under physiological conditions, the luminal domains of RNA-dependent protein kinase-like ER kinase (PERK), IRE1, and ATF6 proteins are occupied by ER resident chaperone BiP/GRP78, which keeps them inactive. When unfolded proteins accumulate in the ER lumen, BiP is released from these complexes to assist with the folding of accumulated unfolded proteins, thus allowing PERK, IRE1, and ATF6 to be activated (Ron and Walter, 2007; Walter and Ron, 2011; Wu and Kaufman, 2006). The activation of these receptors occurs sequentially, with PERK being the first, rapidly followed by ATF6, and IRE1 is activated last. Activated PERK blocks general protein synthesis by phosphorylating eukaryotic initiation factor 2α (eIF2α). ATF6 is activated by limited proteolysis after its translocation from the ER to the Golgi apparatus. Activated ATF6 is also a transcription factor that regulates the expression of ER chaperones (GRP94 and GRP78) and another transcription factor xbp-1. Activated IRE1 protein kinase is required for the splicing of X-box transcription factor 1 (s-xbp1) mRNA, which is subsequently translated into a potent transcription factor. A combination of ATF6 and the spliced variant of xbp1 positively regulate the expression of a wide variety of ER stress target genes, including ER-resident chaperones GRP94 and GRP78 (Ron and Walter, 2007; Walter and Ron, 2011; Wu and Kaufman, 2006). These signaling pathways are referred to as pro-survival unfolded protein responses which try to restore ER function by blocking further protein synthesis, enhancing the folding capacity and initiating degradation of protein aggregates. However, excessive and prolonged ER stress stimulates death signals, which provoke apoptosis and cell death (Hitomi et al., 2004; Nakagawa et al., 2000; Ron and Walter, 2007; Shen et al., 2014; Shimodaira et al., 2014; Szegezdi et al., 2006; Walter and Ron, 2011; Wu and Kaufman, 2006). For instance, CCAAT/enhancer-binding protein–homologous protein (CHOP/GADD153) is a pro-apoptotic protein that can be induced by a combination of the PERK/ATF4 and ATF6 pathways (Shen et al., 2014; Shimodaira et al., 2014; Szegezdi et al., 2006). CHOP over-expression promotes cell death, while deletion of the CHOP gene results in the attenuation of cell death induced by ER stress (Shen et al., 2014; Shimodaira et al., 2014; Szegezdi et al., 2006). ER resident specific protein caspase-12 is activated and involved in ER-stress associated apoptosis (Hitomi et al., 2004; Nakagawa et al., 2000). Additionally, JNK is activated by IRE1-TRAF2-ASK1 during ER stress-induced apoptosis (Urano et al., 2000).

In the present study, we first investigated whether long-term oral exposure to Nano-ZnO caused liver injury, then we studied the potential mechanisms and signaling pathways involved in these effects. We proposed that long-term oral exposure to Nano-ZnO caused oxidative stress and ER stress, which mediated hepatocyte apoptosis, resulting in liver injury and liver function deterioration.

2. Materials and methods

2.1. Preparation and characterization of Nano-ZnO

Nano-ZnO with particle size less than 100 nm were purchased from Sigma-Aldrich (St. Louis, MO, USA). The specific surface area is 15–25 m^2/g, and 79.1–81.5% of Nano-ZnO is Zn by complexometric titration. Nano-ZnO was suspended in physiological saline at a concentration of 25 mg/ml. The stock solution of Nano-ZnO was sonicated at 40 W for 20 minutes and diluted to desired concentrations with physiological saline prior to each experiment. The average hydrodynamic size of Nano-ZnO was measured by dynamic light scattering (DLS) in a zetasizer nano-zs (model ZEN3600), equipped with 4.0 mv 633 nm laser (Malvern Instruments, Malvern, UK).

The shape of Nano-ZnO and the extent of agglomeration in physiological saline were characterized by transmission electron microscopy (TEM). Samples for TEM analysis were prepared by drop coating a solution of Nano-ZnO on carbon-coated copper grids. The films on the TEM grids were dried prior to measurement. TEM measurements were performed on a JEOL model 2100F (Tokyo, Japan) operated at an accelerating voltage of 200 kv.

2.2. Chemicals and reagents

Primary antibodies to p-PERK, p-eIF2α, eIF2α, p-JNK, JNK and GAPDH were obtained from Cell Signaling Technology (Beverly, MA, USA). Anti-CHOP and anti-PERK antibodies were purchased from Sigma-Aldrich (St. Louis, MO, USA). Anti-rabbit secondary antibody was purchased from Santa Cruz Biotechnology (Dallas, TX, USA).

2.3. Animals and treatment

Male C57BL/6 mice (6-week-old, 20 ± 2 g) were obtained from Shanghai Slack Laboratory Animal Company (Shanghai, China). Mice were housed in an airconditioned room (temperature of 20 ± 2 °C, relative humidity of 60 ± 10 %) with a 12-h light and 12-h dark cycle environment and with free access to food and water. The mice were allowed to acclimatize for 3 days before the experiments. The experiments were carried out following protocols approved by the Anima Ethics Committee, College of Medicine, Zhejiang University. All experiments were performed in accordance with the NIH Guide for the Care and Use of Laboratory Animals.

Previous pharmacokinetic studies showed that with oral administration of Nano-ZnO at a dose of 300 mg/kg or less, Nano-ZnO were evenly distributed in tissues and excreted within 24 hours (Baek et al., 2012). In the present study, we randomly assigned mice to two different concentrations of Nano-ZnO, a low dose group (200 mg/kg/day) and a high dose group (400 mg/kg/day), and one vehicle control group (administered physiological saline only). All doses were volumetrically equal (20 ml/kg body weight), and the mice were gavaged once a day for 90 consecutive days.

All mice were observed daily for mortality and clinical signs of toxicity and weighed every other day during the period of the experiment. Before sacrificing, all mice were fasted for 24 hours after the last treatment.

2.4. Biochemical assays in serum

Serum was obtained by centrifugation of blood at 3000 rpm for 15 min. The enzymatic parameters related to liver function, including aspartate aminotransferase (AST) and alanine aminotransferase (ALT), were measured by an automated hematology analyzer (Bayer, PA, USA).

2.5. Coefficient of liver to body weight and liver histopathology

Mice were weighed before sacrifice, and livers were removed, weighed and immediately fixed in 10% neutral buffered formalin. Liver tissues were embedded in paraffin, sectioned at 5 μm, stained with hematoxylin and eosin and observed under light microscopy.

The coefficient of liver to body weight was calculated as the ratio of liver wet weight (mg) to body weight (g).

2.6 Inductively coupled plasma mass spectrometry (ICP-MS)

Zinc concentrations were measured as in previous studies (Becker et al., 2007; Dobrowolska et al., 2008; M-M et al., 2013; Sadauskas et al., 2009). In brief, 1 gram samples of liver tissues were digested for 4 hours at room temperature in 4 ml of 30% nitric acid and 1 ml of H_2O_2, then were digested at 135°C for another 8 hours and analyzed for zinc by ICP-MS. Analytical accuracy was assessed with reagent blanks, initial and continuing calibration verification standards, and standard reference materials. Analytical precision was assessed with sample duplicates.

2.7. ER structure by TEM

Liver tissues were fixed with 2.5% glutaraldehyde in 0.1 mol/dm^3 cacodylate buffer for 2 h, washed three times with 0.1 mol/dm^3 cacodylate buffer and fixed in 1 % osmium tetraoxide for 1h. The tissues were dehydrated by a graded series of ethanol (75, 85, 95 and 100%) and embedded in Epon 812. Ultrathin sections were obtained, stained with uranyl acetate and lead citrate and examined with a HITACHI H600 TEM (HITACHI CO., Japan).

2.8. Enzyme linked immunoasorbent assays (ELISA)

Liver tissue homogenates were prepared by lysing the tissue in 0.1M phosphate buffer (pH 7.4) comprised of 0.1M Na_2HPO_4, 0.1M NaH_2PO_4 and 0.1M KCl, using a Tissuelyser (Qiagen, Germany). After centrifugation (3000 rpm for 10 min at 4°C), the supernatant was assayed for: (1) oxidative stress-related biomarkers, malondialdehyde (MDA) and reduced glutathione (GSH); and (2) apoptosis-related proteins (caspase-3, caspase-9 and caspase-12) with commercial ELISA kits (Nanjing Jiancheng Bioengineering Institute, Jiangsu, China) according to the manufacturer's instructions.

2.9. Real-time PCR

The mRNA expression of ER stress-related genes (grp78, grp94, xbp-1, pdi-3) and apoptosis-related genes (bcl-1, bcl-2, bax, chop) in liver tissues was determined by real-time PCR according to previous reports (Mo et al., 2009; Mo et al., 2012). In brief, total RNA was extracted from liver tissues with Trizol reagent (Qiagen, Germany). The cDNA was

synthesized from 0.5 μg of total RNA with a cDNA synthesis kit (Takara, Dalian, China). All primers (Table 1) were purchased from Haofeng Biotechnology (China). The PCR was performed in duplicate on a CFX-Touch 96 (Bio-Rad, USA) by using SYBR Green PCR Master Mix (Takara, Dalian, China). The reaction parameters for real-time PCR were one cycle at 95°C for 4 min, followed by 40 cycles, with each cycle at 95°C for 5 s, 60°C for 20 s, and 65°C for 30 s. The relative mRNA expression level of the gene was normalized to the level of GAPDH in the same sample.

2.10. Western blot

ER stress-related proteins (PERK, eIF2α, and their phosphorylated proteins) and ER-specific apoptotic proteins (JNK, phosphor-JNK, CHOP) were analyzed by Western blot as previously reported (Mo et al., 2009). Liver homogenates were prepared in a cell lysis buffer with protease and phosphatase inhibitors. After centrifugation (21,000 rpm, 15 min, 4°C), the supernatant was collected for Western blot. The protein concentrations were determined by using the BCA Protein Assay Kit (Beyotime Institute of Biotechnology, China). Equal amounts (50 μg/lane) of total protein were subjected to electrophoresis in a 10% SDS-polyacrylamide gel and transferred onto a polyvinylidene difluoride (PVDF) membrane (Millipore, USA). The membrane was blocked with 5% bovine serum albumin (BSA) in TBST at room temperature for 2 hours and subsequently incubated with primary antibodies (diluted 1:800 to 1:1,000) at 4°C overnight. After washing, the membrane was incubated with horseradish peroxidase-conjugated goat anti-rabbit IgG (Santa Cruz Biotechnology, USA) (diluted 1:5,000) for 1 hour. The membrane was imaged using a Li-Cor Odyssey scanner. Results were quantified using Odyssey 3.0 analytical software (LiCor, Lincoln, NE). The phosphorylated protein (phospho-PERK, phospho-eIF2α, phospho-JNK) expression levels were normalized to their total protein (PERK, eIF2α, JNK) expression levels, while the CHOP expression level was normalized to GAPDH expression level.

2.11. Immunohistochemistry

CHOP, an ER stress-related proapoptotic protein, was also studied by immunohistochemistry in paraffin-embedded liver sections. In brief, slides were deparaffinised, dehydrated and immersed in 1.5% H_2O_2 in methanol for 20 min. For antigen retrieval, slides were incubated in 0.1 M sodium citrate (pH 6) with 0.05% Tween-20 at 100°C for 20 min. Sections were blocked with 5% BSA for 1 h at room temperature and incubated with an anti-CHOP antibody overnight at 4 °C. Slides were subsequently incubated with a secondary antibody for 1 h, and stained with 3,3'-diaminobenzidine (DAB). Sections were counterstained with Mayer’s hematoxylin, mounted and examined under a light microscope. Semi-quantitative analysis was performed on the colored sections using a computer imaging analysis system (Leica QWin V3 image analysis software; Leica Microsystems, Heidelberg, Germany). Briefly, eight to ten digital images were captured randomly from each slide using a 40× objective. CHOP immunostaining were quantified according to the intensity of the color and the percentage of positively stained area. Brown areas were considered as positive. The intensity of the color was graded as 0 (no color); 1 (light yellow); 2 (light brown) and 3 (brown), and the percentage of positively stained area was graded as 0 (<5%); 1 (5–25%); 2 (25–50%); 3 (51–75%) and 4 (>75%). The two grades

were added together to give a final score which represented the extent of CHOP immunostaining.

2.12. Statistical analysis

All values were expressed as mean ± standard deviation (SD). Multi-group comparisons of the means were carried out by one-way analysis of variance (ANOVA) followed by Dunnett's t-test using SPSS 14.0. If a p value was less than 0.05, a difference was considered significant.

3. Results

3.1. Nano-ZnO characterization

The TEM picture of Nano-ZnO is shown in Figure 1A. Nano-ZnO had a polygonal shape with smooth surfaces. The average particle size of Nano-ZnO was 80 nm (Fig. 1A). The mean hydrodynamic size and zeta potential of Nano-ZnO in physiological saline was 223.8 nm and −17.6 mv, respectively by DLS (Fig. 1B).

3.2. Histopathological changes in the liver from mice with oral administration of Nano-ZnO

No toxic signs or mortality were observed in the Nano-ZnO-treated and control mice during the period of the experiments. As shown in Table 2, no significant difference in the body weight of Nano-ZnO-treated mice was observed as compared control mice before and after the experiment. However, the coefficient of liver weight, the ratio of wet liver weight to the mouse body weight, in the Nano-ZnO-treated mice was increased significantly as compared with the controls (Table 2).

Histopathological changes in liver tissues were observed under light microscopy with H&E staining. Focal hepatocellular necrosis and congestive dilated central veins were observed in the liver tissues from mice exposed orally to 200 or 400 mg/kg of Nano-ZnO for 90 days. Normal liver tissue structure was observed in the control mice (Fig. 2).

3.3. Effects of oral administration of Nano-ZnO on liver function

Serum biochemical parameters for liver function of mice following oral administration with Nano-ZnO for 90 consecutive days were determined. Our results showed that AST activity was significantly increased in the serum of mice administered 200 and 400 mg/kg of Nano-ZnO as compared with those in control mice. ALT levels were significantly increased only in mice treated with 200 mg/kg of Nano-ZnO (Table 3). These results indicate a deterioration of liver function in mice exposed to Nano-ZnO orally for 90 days.

3.4. The concentration of zinc in livers from mice after oral administration of Nano-ZnO

The concentration of zinc in liver tissues of mice orally administered Nano-ZnO for 90 consecutive days were determined by ICP-MS. Our results showed that zinc concentrations were significantly increased in liver tissues from mice orally administered 200 and 400 mg/kg of Nano-ZnO as compared with control mice (Table 4).

3.5. Exposure to Nano-ZnO resulted in depletion of GSH in mouse liver tissues

The effects of Nano-ZnO on the production of MDA and depletion of GSH in mouse liver were evaluated by ELISA. Nano-ZnO had a slight but not statistically significant effect on MDA production (Table 5). Oral administration of Nano-ZnO depleted GSH in mouse livers, suggesting that Nano-ZnO caused an imbalance between oxidant and antioxidant systems in the liver (Table 5).

3.6. Effects of Nano-ZnO on ER in hepatocytes

To investigate whether exposure to Nano-ZnO caused direct or indirect damage to the ER structure in hepatocytes, liver tissues were observed under TEM. Exposure to Nano-ZnO resulted in swelling of ER and ribosome degranulation in hepatocytes, while no pathological abnormality was observed in the control mice (Fig. 3), indicating that Nano-ZnO can affect ER structure.

To determine whether oral administration of Nano-ZnO caused ER stress, the mRNA expression of ER stress-associated genes (grp78, grp94, xbp-1, pdi-3) were analyzed by real-time PCR, and ER stress-related protein (p-PERK, PERK, p-eIF2α, eIF2α) expression levels were evaluated by western blot in liver tissues from mice with or without oral administration of Nano-ZnO. Our results demonstrated that the mRNA expression levels of grp78, grp94, xbp-1 and pdi-3 in the liver tissues from mice treated with 200 or 400 mg/kg of Nano-ZnO were significantly higher than those in the control mice (Fig. 4A).

PERK is the major protein responsible for attenuation of mRNA translation under ER stress. Dimerization and transautophosphorylation of PERK activate its kinase activity, leading to phosphorylation of eIF2α and attenuation of mRNA translation and protein synthesis in response to ER stress (Jiang and Wek, 2005). To test whether the effects of Nano-ZnO on ER stress was through the PERK/eIF2α kinase signaling pathway, we determined the protein expression levels of phosphorylated PERK and eIF2α in the liver tissues. Our results showed that Nano-ZnO treatment resulted in a significant increase in phosphorylation of PERK and eIF2α expression as compared with the control mice (Fig. 4 B & C). The above results suggest that oral administration of Nano-ZnO caused ER stress by disruption of ER structure and function in mouse livers.

3.7. Nano-ZnO caused apoptosis in hepatocytes through ER stress

To investigate whether ER stress is involved in Nano-ZnO-induced apoptosis and liver injury, the expression levels of apoptosis-related genes (bcl-1, bcl-2, bax, chop) and proteins (caspase-3, caspase-9, caspase-12, CHOP, JNK) were measured in liver tissues from mice with or without exposure to Nano-ZnO. Our results showed that the mRNA expression levels of pro-apoptotic genes, bax and chop, in the livers of mice treated with Nano-ZnO (200 or 400 mg/kg) were significantly higher than in the control mice (Fig. 5A). 400 mg/kg of Nano-ZnO treatment resulted in a significant decrease in the anti-apoptotic gene bcl-2 mRNA expression in the liver tissues of mice, although 200 mg/kg of Nano-ZnO treatment did not (Fig. 5B). Nano-ZnO did not have any effects on anti-apoptotic gene bcl-1 mRNA expression (Fig. 5B).

Caspases, a family of cysteine proteases, are central regulators of apoptosis. Initiator caspases, such as caspase-12 and casapase-9, are involved in ER stress-initiated apoptotic pathways (Nakagawa et al., 2000; Szegezdi et al., 2003). Caspase-3 is the most important effector caspase (Kuribayashi et al., 2006). In this study, the activities of caspase-3, caspase-9 and caspase-12 in mouse livers were determined by ELISA. The results revealed that the activities of caspase-3, caspase-9 and caspase-12 in the liver tissues from mice treated with Nano-ZnO (200 or 400 mg/kg) were significantly higher than in the control mice (Table 6).

CHOP is known as a crucial factor that mediates ER stress-induced apoptosis (Shen et al., 2014; Szegezdi et al., 2006; Wu and Kaufman, 2006). As shown in Fig. 5A, Nano-ZnO caused *a* significant increase in the mRNA expression level of CHOP in mouse livers. The effects of Nano-ZnO on the expression of CHOP in mouse liver tissues were further investigated by immunohistochemistry staining and Western blot. CHOP positive staining was rare in the liver sections from control mice (Fig. 6 A & D), but was abundant in the livers of mice treated with 200 or 400 mg/kg of Nano-ZnO (Fig. 6 B–D). Western blot results were consistent with the results of immunohistochemistry staining (Fig. 7A and 7B). In addition, Nano-ZnO treatment induced a significant increment in the phosphorylation of JNK (Fig. 8A and 8B). Taken together, these indicate that ER stress-mediated apoptosis is involved in Nano-ZnO-induced liver injury.

4. Discussion

Previous studies demonstrated that zinc has functional properties such as antioxidant, anti-inflammatory and anti-apoptotic effects in addition to its immunoregulatory effects on animals and humans (da Costa et al., 2013). However, a general trend has been shown that toxicity increased as the particulate size decreased. Nano-sized materials may exhibit unknown biological or environmental effects because of their small size and large surface area, even if their bulk counterparts are known to be safe (Yoshida et al., 2009). Nano-ZnO has been commonly used in ceramic manufacture, photocatalysis, UV filters and the food industry (Yon et al., 2011). Nano-ZnO are also used in consumer products such as sunscreen, additives and packing agents due to their antimicrobial properties, and in fungicides, anticancer drugs, and clinical imaging reagents can lead to ingestion exposure (He et al., 2011; Rasmussen et al., 2010). Absorbed Nano-ZnO from the gastrointestinal tract enters the liver through the portal vein and may impact the organ since the liver is the primary organ of metabolism. Therefore, hepatotoxicity is one of the major emerging issues concerning potential hazards of Nano-ZnO. We found that Nano-ZnO was aggregated when it was suspended in physiological saline. However, one of the best-documented properties of nanoparticles is their ability to aggregate, and human exposures will include exposure to aggregated nanoparticles. Therefore, the use of aggregated nanoparticles in toxicology studies is relevant. It is also important to note that toxic effects associated with increased nanoparticle surface area may still occur in aggregated nanoparticles.

ALT and AST, located inside the hepatocytes, are two enzymes by which liver injury can be monitored. When hepatocytes are injured, these enzymes are released into the blood. Thus, increased levels of these enzymes in the blood is a sign of hepatocyte damage. In our study,

oral administration of Nano-ZnO to mice leads to liver injury that was reflected by increased ALT and AST levels in the serum. Nano-ZnO-induced liver injury was further confirmed by histopathological examination, which showed focal hepatocellular necrosis and congestive dilation of central veins. Our findings are consistent with previous studies that showed that oral exposure to Nano-ZnO induced liver injury (Fazilati et al., 2013).

Oxidative stress plays an important role in nanoparticle-induced adverse effects (Kermanizadeh et al., 2012; Shukla et al., 2014). It results from an imbalance between ROS generation and the antioxidant system (enzymatic and not-enzymatic antioxidant). Previous studies have shown that exposure to Nano-ZnO caused oxidative stress *in vitro* and *in vivo* (Chen et al., 2014; Huang et al., 2010; Jo et al., 2013; Sharma et al., 2012a; Sharma et al., 2012b). In our study, although exposure to Nano-ZnO only caused a slight, but not significant increase in MDA contents, Nano-ZnO resulted in a significant decrease in GSH contents in liver tissues. Our findings suggest that oral exposure to Nano-ZnO can deplete antioxidants in the liver, which may further cause an imbalance between oxidants and antioxidants that may result in oxidative stress in the liver.

The endoplasmic reticulum (ER) is an important organelle and functions in folding and assembling cellular proteins, synthesis of lipids and sterols, and storage of free calcium, all of which are dependent on ER internal homeostasis (Roussel et al., 2013). ER stress, also known as unfolded protein response (UPR), is activated upon the accumulation of unfolded proteins in ER lumen or direct ER damage (Ron and Walter, 2007). To investigate whether exposure to Nano-ZnO would cause ER damage directly or indirectly, we examined ER structures in hepatocytes by TEM. The TEM images showed that oral administration of Nano-ZnO to mice resulted in damage to ER structure in hepatocytes, which may lead to ER stress. ER stress is initiated by three ER transmembrane proteins: PERK, IRE1 and ATF6. Under physiological conditions, the luminal domains of the three proteins are occupied by the ER chaperon (GRP78/Bip) which makes them inactive. When ER stress happens, GRP78 dissociates from the three ER transmembrane proteins leading to their activation. PERK is activated by its autophosphorylation and dimerization. Subsequently, PERK phosphorylates the alpha subunit of eukaryotic initiation factor 2 (eIF2α), leading to an attenuation of translation and protein synthesis. Under ER stress, the transcription factor xbp-1 is spliced by the endoribonuclease (RNase) of IRE1, which induces an increased expression level of ER chaperons (grp78, grp94, pdi-3) (Szegezdi et al., 2006). Our results demonstrated a dose-related increase in the mRNA expression of grp78, grp94, xbp-1 and pdi-3 and in the phosphorylation of PERK and eIF2α in liver tissues from mice treated with Nano-ZnO. These results suggest that ER stress occurred in livers of mice after oral exposure to Nano-ZnO.

ER stress usually occurs for a short time in order to recover ER homeostasis for cell survival, but prolonged ER stress activates apoptosis (Hitomi et al., 2004; Szegezdi et al., 2003; Szegezdi et al., 2006; Zhang et al., 2012). ER stress induces apoptosis through several mechanisms, including expression of CHOP, and activation of ER-localized caspases and JNK pathways (Hitomi et al., 2004; Shen et al., 2014; Shimodaira et al., 2014; Szegezdi et al., 2003; Szegezdi et al., 2006; Urano et al., 2000; Zhang et al., 2012). CHOP, is expressed at low levels under physiological conditions, but it is highly expressed in response to ER

stress (Wang et al., 1996). CHOP can induce ER stress-mediated apoptosis through down-regulation of Bcl-2 and depletion of cellular glutathione (McCullough et al., 2001). Our results showed that oral exposure to Nano-ZnO caused increased expression of CHOP in liver tissues. In addition, exposure to Nano-ZnO resulted in up-regulation of pro-apoptotic genes such as bax, and downregulation of anti-apoptotic genes such as bcl-2. These results indicate that activation of CHOP may be involved in Nano-ZnO-induced hepatocyte apoptosis.

Another crucial mechanism involved in ER stress-mediated apoptosis is activation of the JNK pathway. JNK is activated by IRE1 via TRAF2-apoptosis signal regulating kinase-1 (ASK-1). JNK can phosphorylate and activate pro-apoptotic proteins and inactivate anti-apoptotic proteins (Szegezdi et al., 2006; Urano et al., 2000). ER stress promotes also apoptosis through the activation of ER-specific cysteine protease, caspase-12. Caspase-12 is activated by calpains or the interaction with IRE-1 and TRAF-2 (Szegezdi et al., 2003). Following the activation of caspase-12, caspase-3 and caspase-9 are subsequently activated, which induces an apoptotic caspase cascade. Our results demonstrated that exposure to Nano-ZnO caused a significant increase in the phosphorylation of JNK protein and the activity of caspase-3, caspase-9 and caspase-12 in the liver tissues. These results suggest that ER stress may be involved in the Nano-ZnO-induced hepatocyte apoptosis.

In conclusion, we have demonstrated that Nano-ZnO induced oxidative stress and ER stress in the liver, and ER stress-mediated apoptosis, may be involved in Nano-ZnO-induced liver injury. Although the relationship between oxidative stress and ER stress has not been elucidated, these results provide further understanding of the potential hepatotoxic effects caused by oral exposure to metal nanoparticles. The mechanisms by which Nano-ZnO causes oxidative stress, ER stress, apoptosis and liver injury remain important questions that warrant further studies.

Supplementary Material

Refer to Web version on PubMed Central for supplementary material.

Acknowledgements

This work was partly supported by Platform Key Projects of Health and Family Planning Commission of Zhejiang Province to Dr. Mizu Jiang (2012ZDA029), and NIH ES023693 grant funding to Dr. Qunwei Zhang.

Abbreviations

Nano-ZnO	zinc oxide nanoparticles
ER	endoplasmic reticulum
UPR	unfolded protein response
ALT	alanine transaminase
AST	aspartate transaminase
MDA	malondialdehyde

GSH	glutathione
PERK	RNA-dependent protein kinase-like ER kinase
eIF2α	eukaryotic initiation factor 2α
JNK	Jun N-terminal kinase
CHOP	CCAAT/enhancer-binding protein homologous protein
grp78	glucose-regulated protein 78
grp94	glucose-regulated protein 94
pdi-3	protein disulfide isomerase-3
xbp-1	X box-binding protein 1
TEM	transmission electron microscope
SEM	scanning electron microscope
bax	bcl2-associated X protein
bcl-1	cyclin D1
bcl-2	B cell leukemia/lymphoma 2
gapdh	glyceraldehyde-3-phosphate dehydrogenase

References

Akhtar MJ, Ahamed M, Kumar S, Khan MM, Ahmad J, Alrokayan SA. Zinc oxide nanoparticles selectively induce apoptosis in human cancer cells through reactive oxygen species. Int. J. Nanomedicine. 2012; 7:845–857. [PubMed: 22393286]

Aydin Sevinc B, Hanley L. Antibacterial activity of dental composites containing zinc oxide nanoparticles. J. Biomed. Mater. Res. B. Appl. Biomater. 2010; 94:22–31. [PubMed: 20225252]

Baek M, Chung HE, Yu J, Lee JA, Kim TH, Oh JM, Lee WJ, Paek SM, Lee JK, Jeong J, Choy JH, Choi SJ. Pharmacokinetics, tissue distribution, and excretion of zinc oxide nanoparticles. Int. J. Nanomedicine. 2012; 7:3081–3097. [PubMed: 22811602]

Baky NA, Faddah LM, Al-Rasheed NM, Al-Rasheed NM, Fatani AJ. Induction of inflammation, DNA damage and apoptosis in rat heart after oral exposure to zinc oxide nanoparticles and the cardioprotective role of alpha-lipoic acid and vitamin E. Drug Res. (Stuttg). 2013; 63:228–236. [PubMed: 23532625]

Becker JS, Matusch A, Depboylu C, Dobrowolska J, Zoriy MV. Quantitative imaging of selenium, copper, and zinc in thin sections of biological tissues (slugs-genus arion) measured by laser ablation inductively coupled plasma mass spectrometry. Anal. Chem. 2007; 79:6074–6080. [PubMed: 17622184]

Chen R, Huo L, Shi X, Bai R, Zhang Z, Zhao Y, Chang Y, Chen C. Endoplasmic reticulum stress induced by zinc oxide nanoparticles is an earlier biomarker for nanotoxicological evaluation. ACS Nano. 2014; 8:2562–2574. [PubMed: 24490819]

Cho WS, Duffin R, Howie SE, Scotton CJ, Wallace WA, Macnee W, Bradley M, Megson IL, Donaldson K. Progressive severe lung injury by zinc oxide nanoparticles; the role of Zn2+ dissolution inside lysosomes. Part. Fibre. Toxicol. 2011; 8:27. [PubMed: 21896169]

Cho WS, Kang BC, Lee JK, Jeong J, Che JH, Seok SH. Comparative absorption, distribution, and excretion of titanium dioxide and zinc oxide nanoparticles after repeated oral administration. Part. Fibre. Toxicol. 2013; 10:9. [PubMed: 23531334]

Chuang HC, Juan HT, Chang CN, Yan YH, Yuan TH, Wang JS, Chen HC, Hwang YH, Lee CH, Cheng TJ. Cardiopulmonary toxicity of pulmonary exposure to occupationally relevant zinc oxide nanoparticles. Nanotoxicology. 2014; 8:593–604. [PubMed: 23738974]

da Costa CM, Brazao V, Collins Kuehn C, Rodrigues Oliveira LG, do Prado Junior JC, Sala MA, Carraro Abrahao AA. Zinc and pregnancy: Marked changes on the immune response following zinc therapy for pregnant females challenged with Trypanosoma cruzi. Clin. Nutr. 2013; 32:592–598. [PubMed: 23154185]

Dobrowolska J, Dehnhardt M, Matusch A, Zoriy M, Palomero-Gallagher N, Koscielniak P, Zilles K, Becker JS. Quantitative imaging of zinc, copper and lead in three distinct regions of the human brain by laser ablation inductively coupled plasma mass spectrometry. Talanta. 2008; 74:717–723. [PubMed: 18371699]

He L, Liu Y, Mustapha A, Lin M. Antifungal activity of zinc oxide nanoparticles against Botrytis cinerea and Penicillium expansum. Microbiol. Res. 2011; 166:207–215. [PubMed: 20630731]

Hitomi J, Katayama T, Eguchi Y, Kudo T, Taniguchi M, Koyama Y, Manabe T, Yamagishi S, Bando Y, Imaizumi K, Tsujimoto Y, Tohyama M. Involvement of caspase-4 in endoplasmic reticulum stress-induced apoptosis and Abeta-induced cell death. J. Cell Biol. 2004; 165:347–356. [PubMed: 15123740]

Huang CC, Aronstam RS, Chen DR, Huang YW. Oxidative stress, calcium homeostasis, and altered gene expression in human lung epithelial cells exposed to ZnO nanoparticles. Toxicol. In Vitro. 2010; 24:45–55. [PubMed: 19755143]

Jiang HY, Wek RC. Phosphorylation of the alpha-subunit of the eukaryotic initiation factor-2 (eIF2alpha) reduces protein synthesis and enhances apoptosis in response to proteasome inhibition. J. Biol. Chem. 2005; 280:14189–14202. [PubMed: 15684420]

Jo E, Seo G, Kwon JT, Lee M, Lee B, Eom I, Kim P, Choi K. Exposure to zinc oxide nanoparticles affects reproductive development and biodistribution in offspring rats. J. Toxicol. Sci. 2013; 38:525–530. [PubMed: 23824008]

Kermanizadeh A, Gaiser BK, Hutchison GR, Stone V. An in vitro liver model--assessing oxidative stress and genotoxicity following exposure of hepatocytes to a panel of engineered nanomaterials. Part. Fibre. Toxicol. 2012; 9:28. [PubMed: 22812506]

Kuribayashi K, Mayes PA, El-Deiry WS. What are caspases 3 and 7 doing upstream of the mitochondria? Cancer Biol. Ther. 2006; 5:763–765. [PubMed: 16921264]

M-M P, Weiskirchen R, Gassler N, Bosserhoff AK, Becker JS. Novel bioimaging techniques of metals by laser ablation inductively coupled plasma mass spectrometry for diagnosis of fibrotic and cirrhotic liver disorders. PLoS One. 2013; 8:e58702. [PubMed: 23505552]

Malhi H, Kaufman RJ. Endoplasmic reticulum stress in liver disease. J. Hepatol. 2011; 54:795–809. [PubMed: 21145844]

McCullough KD, Martindale JL, Klotz LO, Aw TY, Holbrook NJ. Gadd153 sensitizes cells to endoplasmic reticulum stress by down-regulating Bcl2 and perturbing the cellular redox state. Mol. Cell Biol. 2001; 21:1249–1259. [PubMed: 11158311]

Michalak M. Quality control in the endoplasmic reticulum. Semin. Cell Dev. Biol. 2010; 21:471. [PubMed: 20304087]

Mo Y, Wan R, Chien S, Tollerud DJ, Zhang Q. Activation of endothelial cells after exposure to ambient ultrafine particles: the role of NADPH oxidase. Toxicol. Appl. Pharmacol. 2009; 236:183–193. [PubMed: 19371610]

Mo Y, Wan R, Zhang Q. Application of reverse transcription-PCR and real-time PCR in nanotoxicity research. Methods Mol. Biol. 2012; 926:99–112. [PubMed: 22975959]

Nakagawa T, Zhu H, Morishima N, Li E, Xu J, Yankner BA, Yuan J. Caspase-12 mediates endoplasmic-reticulum-specific apoptosis and cytotoxicity by amyloid-beta. Nature. 2000; 403:98–103. [PubMed: 10638761]

Pasupuleti S, Alapati S, Ganapathy S, Anumolu G, Pully NR, Prakhya BM. Toxicity of zinc oxide nanoparticles through oral route. Toxicol. Ind. Health. 2012; 28:675–686. [PubMed: 22033421]

Premanathan M, Karthikeyan K, Jeyasubramanian K, Manivannan G. Selective toxicity of ZnO nanoparticles toward Gram-positive bacteria and cancer cells by apoptosis through lipid peroxidation. Nanomedicine. 2011; 7:184–192. [PubMed: 21034861]

Rasmussen JW, Martinez E, Louka P, Wingett DG. Zinc oxide nanoparticles for selective destruction of tumor cells and potential for drug delivery applications. Expert Opin. Drug Deliv. 2010; 7:1063–1077. [PubMed: 20716019]

Ron P, Walter P. Signal integration in the endoplasmic reticulum unfolded protein response. Nat. Rev. Mol. Cell Biol. 2007; 8:519–529. [PubMed: 17565364]

Roussel BD, Kruppa AJ, Miranda E, Crowther DC, Lomas DA, Marciniak SJ. Endoplasmic reticulum dysfunction in neurological disease. Lancet Neurol. 2013; 12:105–118. [PubMed: 23237905]

Sadauskas E, Danscher G, Stoltenberg M, Vogel U, Larsen A, Wallin H. Protracted elimination of gold nanoparticles from mouse liver. Nanomedicine. 2009; 5:162–169. [PubMed: 19217434]

Schilling K, Bradford B, Castelli D, Dufour E, Nash JF, Pape W, Schulte S, Tooley I, van den Bosch J, Schellauf F. Human safety review of "nano" titanium dioxide and zinc oxide. Photochem. Photobiol. Sci. 2010; 9:495–509. [PubMed: 20354643]

Seok SH, Cho WS, Park JS, Na Y, Jang A, Kim H, Cho Y, Kim T, You JR, Ko S, Kang BC, Lee JK, Jeong J, Che JH. Rat pancreatitis produced by 13-week administration of zinc oxide nanoparticles: biopersistence of nanoparticles and possible solutions. J. Appl. Toxicol. 2013; 33:1089–1096. [PubMed: 23408656]

Service RF. American Chemical Society meeting. Nanomaterials show signs of toxicity. Science. 2003; 300:243.

Sharma V, Anderson D, Dhawan A. Zinc oxide nanoparticles induce oxidative DNA damage and ROS-triggered mitochondria mediated apoptosis in human liver cells (HepG2). Apoptosis. 2012a; 17:852–870. [PubMed: 22395444]

Sharma V, Singh P, Pandey AK, Dhawan A. Induction of oxidative stress, DNA damage and apoptosis in mouse liver after sub-acute oral exposure to zinc oxide nanoparticles. Mutat. Res. 2012b; 745:84–91. [PubMed: 22198329]

Shen M, Wang L, Yang G, Gao L, Wang B, Guo X, Zeng C, Xu Y, Shen L, Cheng K, Xia Y, Li X, Wang H, Fan L, Wang X. Baicalin protects the cardiomyocytes from ER stress-induced apoptosis: inhibition of CHOP through induction of endothelial nitric oxide synthase. PLoS One. 2014; 9:e88389. [PubMed: 24520378]

Shimodaira Y, Takahashi S, Kinouchi Y, Endo K, Shiga H, Kakuta Y, Kuroha M, Shimosegawa T. Modulation of endoplasmic reticulum (ER) stress-induced autophagy by C/EBP homologous protein (CHOP) and inositol-requiring enzyme 1alpha (IRE1alpha) in human colon cancer cells. Biochem. Biophys. Res. Commun. 2014; 445:524–533. [PubMed: 24565834]

Shukla RK, Kumar A, Vallabani NV, Pandey AK, Dhawan A. Titanium dioxide nanoparticle-induced oxidative stress triggers DNA damage and hepatic injury in mice. Nanomedicine (Lond). 2014; 9:1423–1434. [PubMed: 24367968]

Su YK, Peng SM, Ji LW, Wu CZ, Cheng WB, Liu CH. Ultraviolet ZnO nanorod photosensors. Langmuir. 2010; 26:603–606. [PubMed: 19894681]

Szegezdi E, Fitzgerald U, Samali A. Caspase-12 and ER-stress-mediated apoptosis: the story so far. Ann. N. Y. Acad. Sci. 2003; 1010:186–194. [PubMed: 15033718]

Szegezdi E, Logue SE, Gorman AM, Samali A. Mediators of endoplasmic reticulum stress-induced apoptosis. EMBO Rep. 2006; 7:880–885. [PubMed: 16953201]

Umrani RD, Paknikar KM. Zinc oxide nanoparticles show antidiabetic activity in streptozotocin-induced Type 1 and 2 diabetic rats. Nanomedicine (Lond). 2014; 9:89–104. [PubMed: 23427863]

Urano F, Wang X, Bertolotti A, Zhang Y, Chung P, Harding HP, Ron D. Coupling of stress in the ER to activation of JNK protein kinases by transmembrane protein kinase IRE1. Science. 2000; 287:664–666. [PubMed: 10650002]

Walter P, Ron D. The unfolded protein response: from stress pathway to homeostatic regulation. Science. 2011; 334:1081–1086. [PubMed: 22116877]

Wang B, Feng WY, Wang TC, Jia G, Wang M, Shi JW, Zhang F, Zhao YL, Chai ZF. Acute toxicity of nano- and micro-scale zinc powder in healthy adult mice. Toxicol. Lett. 2006; 161:115–123. [PubMed: 16165331]

Wang XZ, Lawson B, Brewer JW, Zinszner H, Sanjay A, Mi LJ, Boorstein R, Kreibich G, Hendershot LM, Ron D. Signals from the stressed endoplasmic reticulum induce C/EBP-homologous protein (CHOP/GADD153). Mol. Cell Biol. 1996; 16:4273–4280. [PubMed: 8754828]

Wu J, Kaufman RJ. From acute ER stress to physiological roles of the Unfolded Protein Response. Cell Death Differ. 2006; 13:374–384. [PubMed: 16397578]

Yoshida R, Kitamura D, Maenosono S. Mutagenicity of water-soluble ZnO nanoparticles in Ames test. J. Toxicol. Sci. 2009; 34:119–122. [PubMed: 19182441]

Zhang R, Piao MJ, Kim KC, Kim AD, Choi JY, Choi J, Hyun JW. Endoplasmic reticulum stress signaling is involved in silver nanoparticles-induced apoptosis. Int. J. Biochem. Cell Biol. 2012; 44:224–232. [PubMed: 22064246]

Highlights

- Administration orally with ZnO nanoparticles (Nano-ZnO) caused disruption of ER structure and function in hepatocytes, resulting in ER stress.
- Nano- ZnO also caused ER stress-associated genes and proteins upregulation and hepatocyte apoptosis.
- ER stress may be involved in Nano-ZnO-induced liver injury.

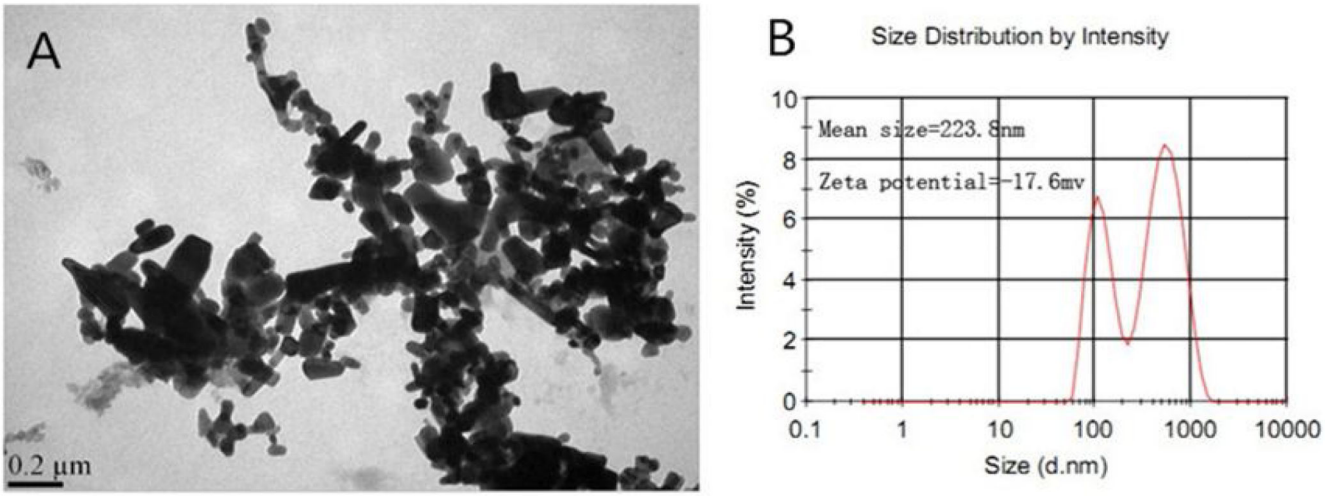

Fig. 1. Characterization of Nano-ZnO

(A) TEM image. (B) Size distribution and zeta potential of Nano-ZnO measured by dynamic light scattering (DLS).

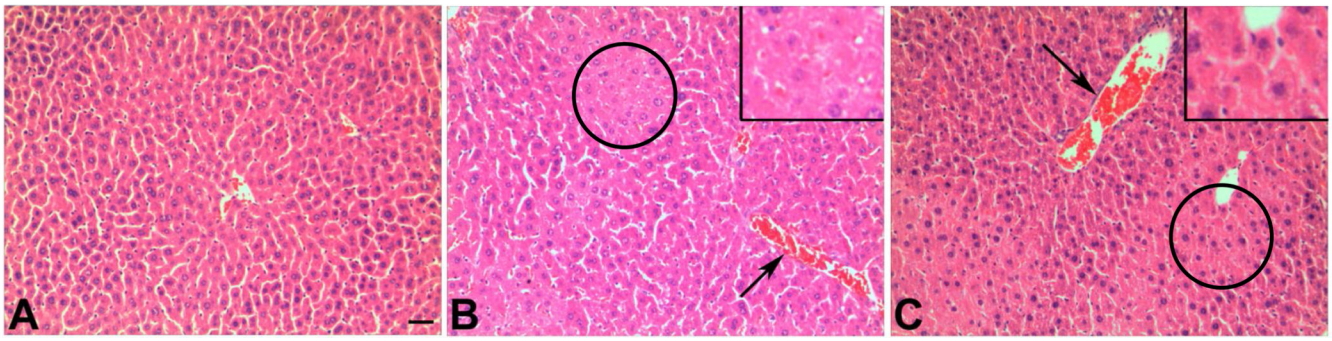

Fig. 2. Histopathology of mouse liver tissue

Liver sections from mice orally administrated physiological saline (A), 200 mg/kg (B), or 400 mg/kg (C) of Nano-ZnO for 90 consecutive days were stained with hematoxylin and eosin. A shows normal liver structure in control mice, while B and C show focal necrosis (circles) and congestive dilated central veins (arrows) in the liver tissue from mice treated with Nano-ZnO. Inserts in B and C are enlarged focal necrosis areas. Scale bar in A indicates 50 μm for all panels.

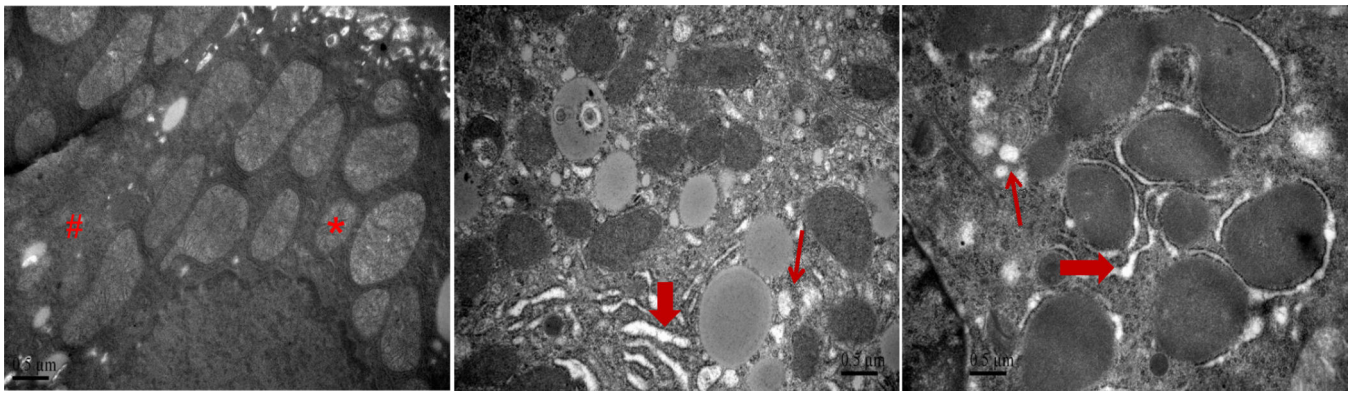

Fig. 3. TEM images of hepatocytes

Mice were orally administrated physiological saline (A), 200 mg/kg (B), or 400 mg/kg (C) of Nano-ZnO for 90 consecutive days. Hepatocytes were observed under TEM. Normal control hepatocyte ultrastructure with normal mitochondria (*) and ER (#) are shown in A. Swelling of endoplasmic reticulum (thick arrows in B and C) and ribosome degranulation (thin arrows in B and C) were observed in hepatocytes of mice treated with Nano-ZnO. Scale bars indicate 0.5 μm.

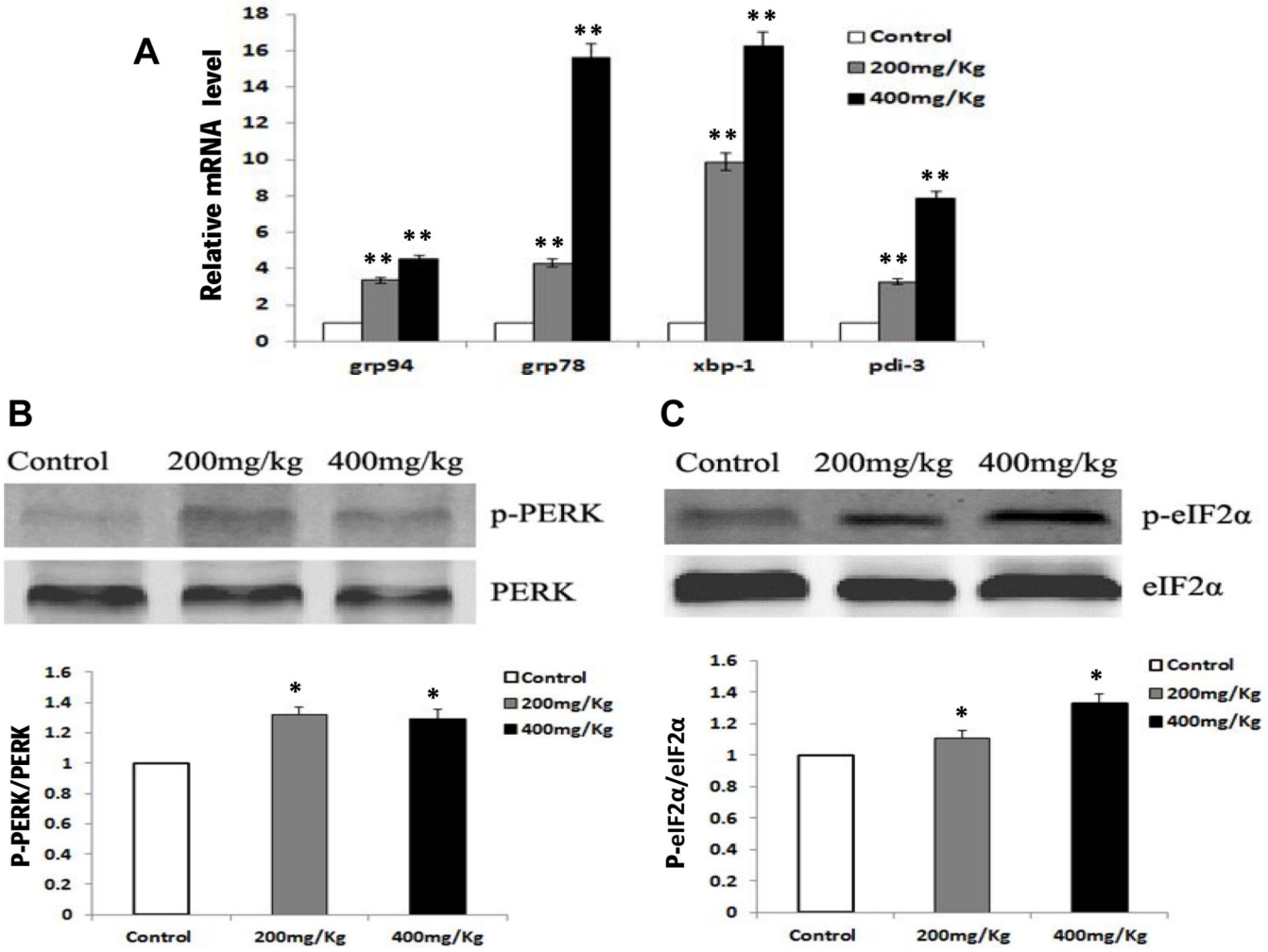

Fig. 4. The effects of Nano-ZnO on ER stress-related markers

Mice were orally administrated physiological saline (control), 200 mg/kg, or 400 mg/kg of Nano-ZnO for 90 consecutive days. The mRNA expression levels of grp94, grp78, xbp-1 and pdi-3 in mouse livers were analyzed by real-time PCR (A). Values are expressed as mean ± SD (n = 6–8). ** $p<0.01$ vs. Control. The expression levels of phosphorylated PERK (p-PERK) and phosphorylated elF2a (p-eIF2a) were determined by Western blot (B and C). Upper panel, representative Western blot results; lower panel, average band densities normalized with their relative total protein. Values are expressed in arbitrary units as mean ± SD (n = 6–8). * $p<0.05$ vs. Control.

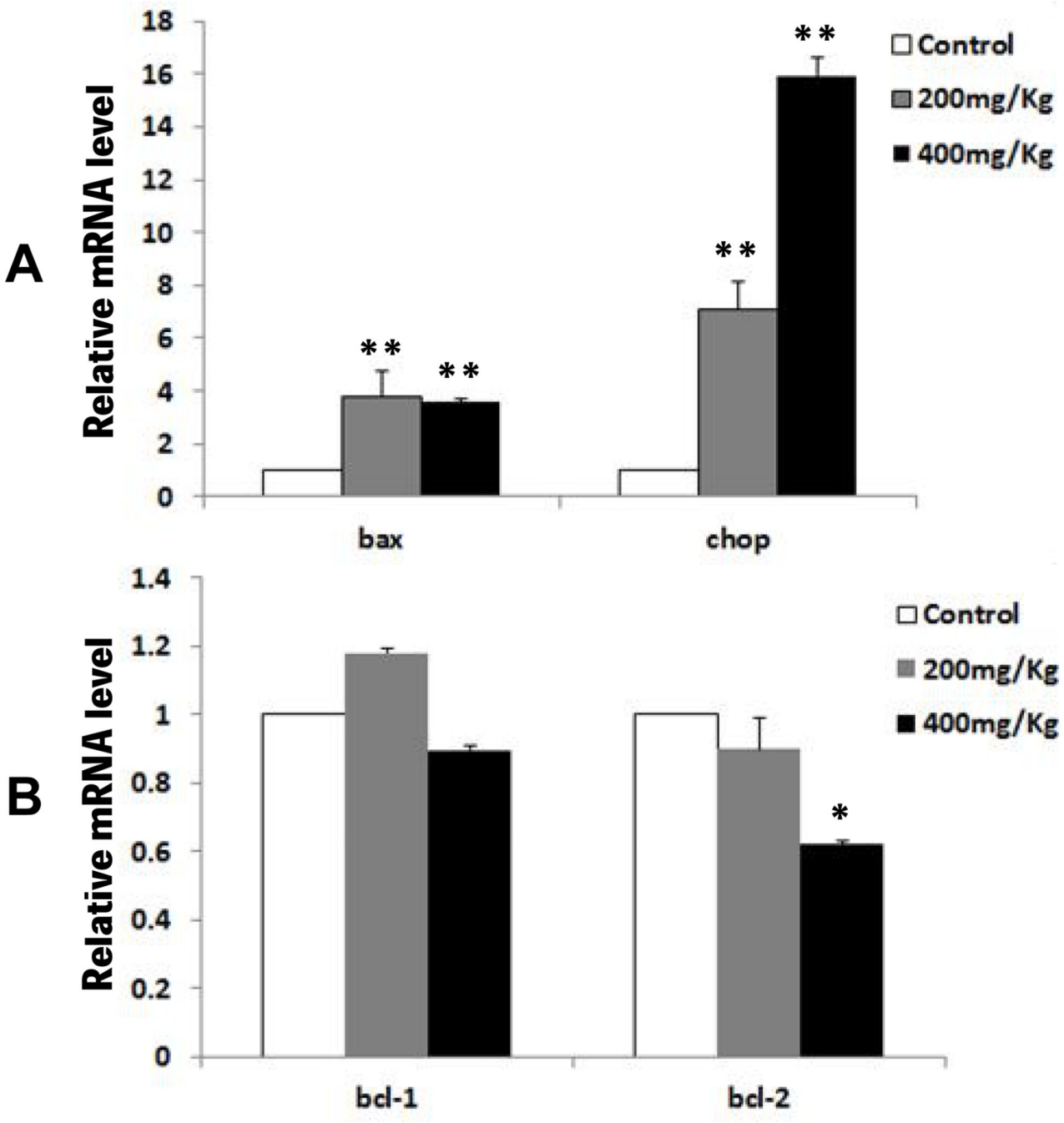

Fig. 5. The effects of Nano-ZnO on mRNA expression levels of apoptosis-related genes

Mice were orally administrated physiological saline (control), 200 mg/kg, or 400 mg/kg of Nano-ZnO for 90 consecutive days. The mRNA expression levels of bax, chop, bcl-1 and bcl-2 were determined in the mouse livers by real-time PCR. Values are expressed as mean ± SD (n=6–8). * $p<0.05$ vs. control; ** $p<0.01$ vs. control.

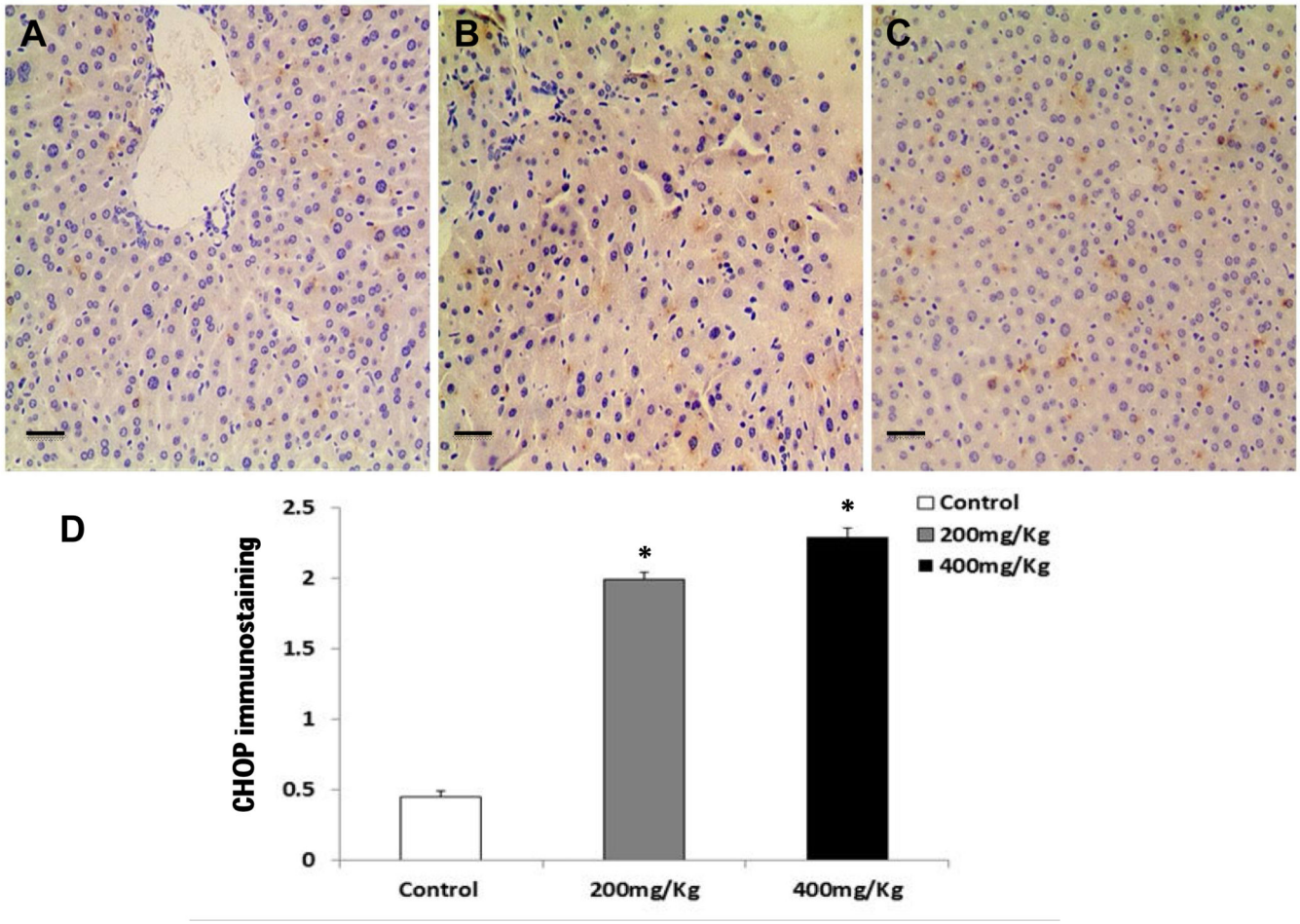

Fig. 6. Immunohistochemistry staining for CHOP protein in the livers of mice treated with Nano-ZnO

Mice were orally administrated physiological saline (A, control), 200 mg/kg (B), or 400 mg/kg (C) of Nano-ZnO for 90 consecutive days. (A–C) Liver sections were stained immunohistochemically for the ER-associated apoptosis-related protein CHOP. The brown granules in the nucleus and cytoplasm indicate the presence of CHOP. Scale bars in A–C indicate 50 μm. (D) Semi-quantitative analysis of immunohistochemical staining of CHOP in the livers as described in the Materials and Methods. Values are expressed as mean ± SD (n=6–8). * $p<0.05$ vs. control.

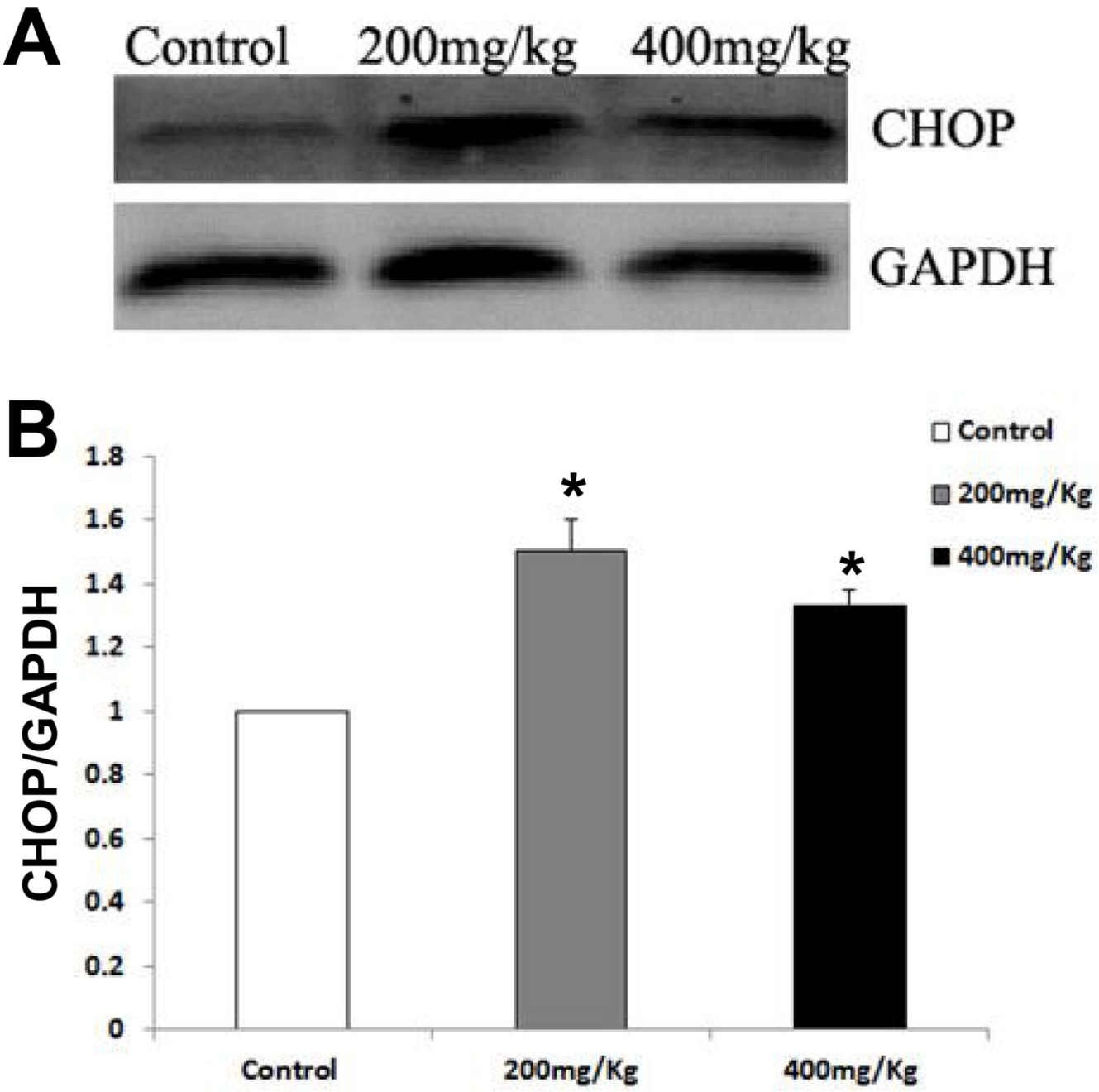

Fig. 7. Western blot analysis for CHOP protein in the livers of mice treated with Nano-ZnO

Mice were orally administrated physiological saline (control), 200 mg/kg, or 400 mg/kg of Nano-ZnO for 90 consecutive days. The protein expression level of CHOP was determined in mouse liver homogenates by Western blot. A is a representative Western blot result, while B shows average band densities normalized with GAPDH. Values are expressed as mean ± SD (n=6–8). * $p<0.05$ vs. control.

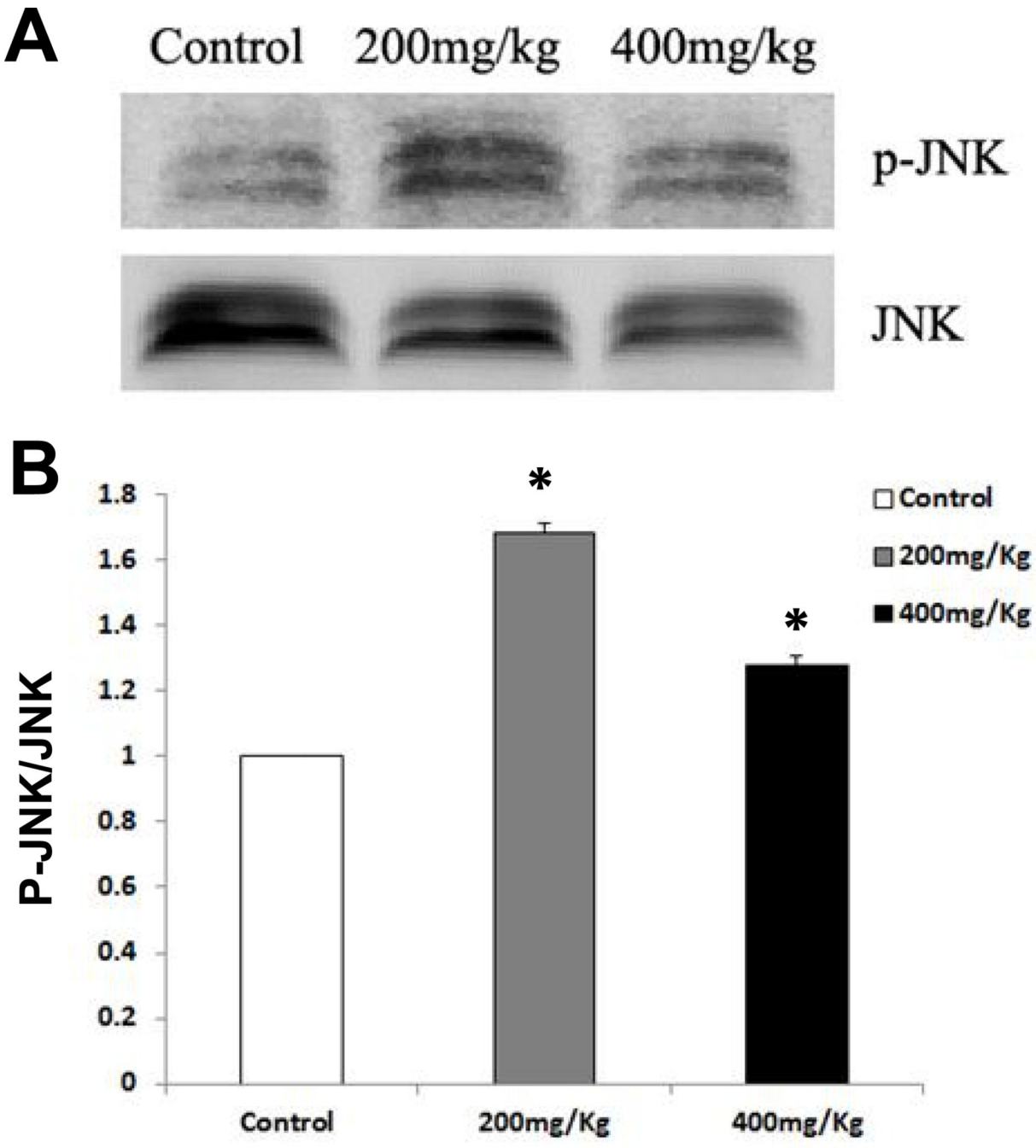

Fig. 8. The effects of Nano-ZnO on the phosphorylation of JNK

Mice were orally administrated physiological saline (control), 200 mg/kg, or 400 mg/kg of Nano-ZnO for 90 consecutive days. The phosphorylation of JNK (p-JNK) was determined in mouse liver homogenates by Western blot. A is a representative Western blot result, while B shows average band densities normalized with total JNK. Values are expressed as mean ± SD (n=6–8). * $p<0.05$ vs. control.

Table 1

Primers for real-time PCR.

Gene	Forward (5’ → 3’)	Reverse (5’ → 3’)
xbp-1	CAGCAAGTGGTGGATTTGGAAG	TCTTAACTCCTGGTTCTCAACCACA
chop	AATAACAGCCGGAACCTGAGGA	ACTCAGCTGCCATGACTGCAC
pdi-3	GGCAAGGACTTACTCACCGCTTAC	CAAAGTTGAGTTTGTGTCCAGCATC
grp78	TGCGGCCAAGAACCAACTC	AATGTCTTGGTTTGCCCACCTC
grp94	TGCCACAACTCATACAGCTGAGTC	ACTTGTTGAAGCCCTGCATCC
bax	CAGGATGCGTCCACCAAGAA	CGTGTCCACGTCAGCAATCA
bcl-1	TACCGCACAACGCACTTTC	AAGGGCTTCAATCTGTTCCTG
bcl-2	AACATCGCCCTGTGGATGAC	CAGGGTCTTCAGAGACAGCCAG
gapdh	AAATGGTGAAGGTCGGTGTGAAC	CAACAATCTCCACTTTGCCACTG

Table 2

Body weight and liver coefficient of mice after oral administration with Nano-ZnO for 90 consecutive days.

Groups	Body weight (g)		Liver coefficient (mg/g)
	Before	After	
Control	22.07 ± 0.80	28.48 ± 3.55	30.03 ± 3.72
Nano-ZnO (200 mg/kg)	21.95 ± 0.79	26.37 ± 3.48	36.40 ± 5.29*
Nano-ZnO (400 mg/kg)	22.62 ± 0.73	27.65 ± 2.21	35.04 ± 4.08*

Values represent mean ± SD (n=10).

* $p<0.05$ vs. control.

Table 3

Serum biochemical parameters in mice after oral administration with Nano-ZnO for 90 consecutive days.

Groups	ALT (U/L)	AST (U/L)
Control	29.8 ± 5.1	89.3 ± 4.9
Nano-ZnO (200 mg/kg)	50.2 ± 16.8 *	146.8 ± 33.8 *
Nano-ZnO (400 mg/kg)	40.0 ± 15.6	132.6 ± 16.6 *

Values represent mean ± SD (n=10).

* $p<0.05$ vs. control.

Table 4

The zinc concentrations in liver tissues from mice administrated orally with Nano-ZnO for 90 consecutive days measured by ICP-MS.

Groups	Zinc concentrations (μg/g liver tissue)
Control	256.89 ± 20.24
Nano-ZnO (200 mg/kg)	532.61 ± 47.67 **
Nano-ZnO (400 mg/kg)	463.56 ± 36.56 **

Values represent mean ± SD (n=10).

** $p<0.01$ vs. control.

Table 5

Oxidative stress parameters in liver tissues from mice after oral administration with Nano-ZnO for 90 consecutive days.

Groups	MDA (μmol/g protein)	GSH (mg/g protein)
Control	3.11 ± 0.77	1.85 ± 0.56
Nano-ZnO (200 mg/kg)	3.68 ± 0.66	1.03 ± 0.42**
Nano-ZnO (400 mg/kg)	4.06 ± 1.87	0.79 ± 0.24**

Values represent mean ± SD (n=10).

** $p<0.01$ vs. control.

Table 6

The activities of caspase-3, caspase-9, and caspase-12 in liver tissues from mice administrated orally with Nano-ZnO for 90 consecutive days.

Group	Caspase-3 (ng/ml)	Caspase-9 (ng/ml)	Caspase-12 (ng/ml)
Control	1.072 ± 0.212	1.053 ± 0.194	541.41 ± 68.39
Nano-ZnO(200 mg/kg)	1.433 ± 0.293*	1.325 ± 0.138*	702.15 ± 59.39*
Nano-ZnO(400 mg/kg)	1.497 ± 0.271*	1.331 ± 0.214*	780.46 ± 111.16*

Values represent mean ± SD (n=10).

* $p<0.05$ vs. control.